Anthrahydroquinone-2,6-disulfonate attenuates PQ-induced acute lung injury through decreasing pulmonary microvascular permeability via inhibition of the PI3K/AKT/eNOS pathway

NAN LI[1-3*], YANG YI[1-3*], JUN CHEN[4*], YUE HUANG[1-3], JICHAO PENG[1], ZHAO LI[1-3], YING WANG[1-3], JIADONG ZHANG[1-3], CHAOQUN XU[1-3], HAORAN LIU[1-3], JINGHUA LI[1-3] and XIAORAN LIU[1-3]

[1]College of Emergency Trauma, Hainan Medical University, Haikou, Hainan 571199, P.R. China; [2]Key Laboratory of Hainan Trauma and Disaster Rescue, The First Affiliated Hospital of Hainan Medical University, Haikou, Hainan 570102, P.R. China; [3]Key Laboratory of Emergency and Trauma Ministry of Education, Hainan Medical University, Haikou, Hainan 571199, P.R. China; [4]Emergency Department of Danzhou People's Hospital, Danzhou, Hainan 571799, P.R. China

Received March 2, 2024; Accepted May 24, 2024

DOI: 10.3892/ijmm.2024.5387

Abstract. In paraquat (PQ)-induced acute lung injury (ALI)/acute respiratory distress syndrome, PQ disrupts endothelial cell function and vascular integrity, which leads to increased pulmonary leakage. Anthrahydroquinone-2,6-disulfonate (AH_2QDS) is a reducing agent that attenuates the extent of renal injury and improves survival in PQ-intoxicated Sprague-Dawley (SD) rats. The present study aimed to explore the beneficial role of AH_2QDS in PQ-induced ALI and its related mechanisms. A PQ-intoxicated ALI model was established using PQ gavage in SD rats. Human pulmonary microvascular endothelial cells (HPMECs) were challenged with PQ. Superoxide dismutase, malondialdehyde, reactive oxygen species and nitric oxide (NO) fluorescence were examined to detect the level of oxidative stress in HPMECs. The levels of TNF-α, IL-1β and IL-6 were assessed using an ELISA. Transwell and Cell Counting Kit-8 assays were performed to detect the migration and proliferation of the cells. The pathological changes in lung tissues and blood vessels were examined by haematoxylin and eosin staining. Evans blue staining was used to detect pulmonary microvascular permeability. Western blotting was performed to detect target protein levels. Immunofluorescence and immunohistochemical staining were used to detect the expression levels of target proteins in HPMECs and lung tissues. AH_2QDS inhibited inflammatory responses in lung tissues and HPMECs, and promoted the proliferation and migration of HPMECs. In addition, AH_2QDS reduced pulmonary microvascular permeability by upregulating the levels of vascular endothelial-cadherin, zonula occludens-1 and CD31, thereby attenuating pathological changes in the lungs in rats. Finally, these effects may be related to the suppression of the phosphatidylinositol-3-kinase (PI3K)/protein kinase B (AKT)/endothelial-type NO synthase (eNOS) signalling pathway in endothelial cells. In conclusion, AH_2QDS ameliorated PQ-induced ALI by improving alveolar endothelial barrier disruption via modulation of the PI3K/AKT/eNOS signalling pathway, which may be an effective candidate for the treatment of PQ-induced ALI.

Correspondence to: Professor Jinghua Li or Professor Xiaoran Liu, College of Emergency Trauma, Hainan Medical University, 3 Xueyuan Road, Haikou, Hainan 571199, P.R. China
E-mail: anubiss1860@163.com
E-mail: hy0203049@hainmc.edu.cn

*Contributed equally

Abbreviations: PQ, paraquat; AH_2QDS, anthrahydroquinone-2,6-disulfonate; SD, Sprague-Dawley; ALI, acute lung injury; ARDS, acute respiratory distress syndrome; SOD, superoxide dismutase; MDA, malondialdehyde; ROS, reactive oxygen species; PI3K, phosphatidylinositol-3-kinase; AKT, protein kinase B; NO, nitric oxide; eNOS, endothelial-type NO synthase; TJs, tight junctions; AJs, adherens junctions; IL, interleukin; TNF tumor necrosis factor; H&E, haematoxylin and eosin staining; WB, western blotting; ELISA, enzyme-linked immunosorbent assay; PBS, phosphate-buffered saline; TBST, Tris-buffered saline with Tween-20

Key words: ALI/ARDS, AH_2QDS, pulmonary microvascular permeability, PQ, PI3K/AKT/eNOS pathway

Introduction

Paraquat (PQ; 1,1-dimethyl-4,4-bipyridinium dichloride) is an effective herbicide that is widely used in agriculture and is highly toxic to humans (1). As of 2020, >150,000 individuals will succumb each year to accidental or intentional exposure to PQ (2). When PQ is absorbed into the body it can cause damage to the lungs, liver, kidneys, heart and other organs (3,4). The lungs have a strong dopamine uptake system to the extent that PQ, which is chemically similar to polyamines, accumulates mainly in the lungs (5). Therefore, when PQ is absorbed into the bloodstream, it directly causes damage to vascular endothelial cells. It has been demonstrated that PQ exposure induces glutathione redox cycle dysfunction and excessive endothelial albumin permeability in microvascular

endothelial cells (6,7). Therefore, identification of therapeutic agents that can maintain the endothelial barrier and attenuate pulmonary microvascular permeability may reduce mortality and improve prognosis, which is of great significance for the clinical treatment of PQ-induced acute lung injury (ALI), but its protective mechanism needs further study. Endothelial cells, the basic building blocks of blood vessels, are involved in and regulate a variety of physiological processes, such as blood and component transport, immune responses and vascular tone (8,9). Multiple causes of endothelial dysfunction accelerate the progression of ALI/acute respiratory distress syndrome (ARDS) (10). It has been demonstrated that vascular endothelial injury can lead to damage to the alveolar-capillary barrier, which in turn leads to increased pulmonary microvascular permeability. The structures of tight junctions (TJs) or adherens junctions (AJs) maintain the integrity of the endothelial barrier (11,12). In ARDS, there is increased permeability of the pulmonary vasculature to circulating fluids, macromolecules and leukocytes due to a severe inflammatory response that disrupts the endothelial barrier, leading to alveolar filling and neutrophilic in-flow. This leads to the high mortality rate of ARDS (13-15).

Anthrahydroquinone-2,6-disulfonate (AH_2QDS) is a reducing agent that has previously been demonstrated to bind specifically to PQ to reduce its levels in the body and thereby improve its survival (16-19). Additionally, it has been demonstrated that AH_2QDS has a protective effect on the kidney in PQ poisoning (20), and this protective mechanism may be related to cellular oxidative stress, inflammatory injury, endoplasmic reticulum stress and reduced apoptosis; however, its mechanism of action in ALI has not been elucidated.

As an important signal transduction pathway in cells, the phosphatidylinositol-3-kinase (PI3K)/protein kinase B (AKT) signalling pathway is involved in a variety of biological processes, such as proliferation, differentiation and anti-inflammatory processes (21,22). It has been demonstrated that endothelial-type nitric oxide (NO) synthase (eNOS) is a key regulator of vascular growth and endothelial function, and can cause relevant biological effects in endothelial cells and airway epithelial cells, affecting the course of ALI/ARDS (23). NO can be generated by eNOS catalysis. The excessive generation of NO can induce the generation of oxygen free radicals, leading to tissue and organ damage, which serves an important role in the pathophysiology of PQ-intoxicated (24,25). To delve deeply into the critical signaling pathway that PQ induces ALI, Sprague-Dawley (SD) rats were utilized to establish a PQ poisoning model and these rats were carefully divided into control, PQ poisoning and AH_2QDS treatment groups. Through detailed comparative analysis with reference genes, enrichment analysis at the gene expression level was conducted. The Kyoto Encyclopedia of Genes and Genomes (KEGG) pathway enrichment analysis revealed that the PI3K/AKT signaling pathway exhibited a particularly significant gene enrichment phenomenon in lung tissues after PQ poisoning and AH_2QDS treatment, indicating that it may be the primary signaling pathway (19,26). Furthermore, according to current understanding, the specific mechanism of the PI3K/AKT/eNOS signaling pathway in the protective effect of AH_2QDS against PQ-induced ALI remains unclear, which precisely constitutes the focus and core of our current study.

In the present study, PQ gavage in rats and PQ treatment of human pulmonary microvascular endothelial cells (HPMECs) were used as *in vitro* and *in vivo* models to validate the aforementioned hypothesis. The results suggested that AH_2QDS could enhance the proliferation and migration of HPMECs. In addition, AH_2QDS reduced inflammatory response and pulmonary microvascular permeability through inactivating the PI3K/AKT/eNOS pathway, thereby attenuating PQ-induced ALI.

Materials and methods

Establishment of the ALI model. A total of 48 male SD rats (7-8 weeks old) with an average weight of 180-200 g were obtained from Changsha Tianqin Biotechnology Co., Ltd., and the rats were kept at Hainan Medical University's Experimental Animal Center using specific pathogen-free standards, with free access to water and food. The animal room was maintained at 22-24˚C with a 12/12-h light-dark cycle. All animal experiments are conducted in the Experimental Animal Center of Hainan Medical University. The rats were randomly divided into the following four groups (n=12) after 7 days of acclimation feeding: Control group, PQ group, PQ + AH_2QDS group and AH_2QDS group (20). To model the poisoning, rats were fasted for 10 h prior to poisoning with reference to previous experiments (19,20). The control group was given 5 ml saline by gavage. The PQ group was administered 200 mg/kg 20% PQ solution per rat by gavage (Henan Lane Pesticide Factory). The PQ + AH_2QDS group was given 5 ml AH_2QDS by gavage at the molar ratio of PQ:AH_2QDS=1:1 (mol:mol) after 2 h of PQ intoxication, which was used to construct the treatment model. The AH_2QDS group was administered 5 ml AH_2QDS by gavage. To adhere to the principle of humane endpoints, the following measures were taken during the experiment to minimize the use of animals while ensuring the scientific rigor and humanity of the experiment. Firstly, sufficient practice was conducted and the modelling techniques were mastered beforehand to significantly reduce the failure rate of animal modelling, thus ensuring the reliability and validity of the experimental results. Secondly, during all experimental operations, it was ensured that animals were anesthetized to minimize potential pain and discomfort during the experiment. In addition, strict adherence to experimental ethical norms was implemented and clear humanitarian endpoints were formulated, tailored to the objectives of the present study. The specific standards were as follows: i) After 72 h of PQ intervention, as the scientific goals of the research were achieved, there was no need to continue the experiment; ii) when animals suffered from pain that was not caused by the experiment itself and was unexpected before the experiment starts, such as animals with inherent defects; iii) if it was anticipated before the experiment that the animals may suffer from pain, but the degree of pain exceeded expectations during the actual process, such as severe nasal and oral bleeding, severely abnormal behaviour, and other situations; and iv) if the pain of the animals was caused by the experiment itself, and this pain had been anticipated before the experiment started. Once any of the aforementioned standards were observed during the experiment, the animals were immediately euthanized to reduce their suffering. All animals in the present study were

euthanized before the end of the experiment once these standards were met, ensuring that no animals would succumb due to any unnecessary reasons during the experimental process. The animal welfare was always upheld and the smooth progress of the experiment was ensured while maintaining the accuracy and reliability of the experimental results. The rats were euthanized using an overdose of sodium pentobarbital (>150 mg/kg) injected intraperitoneally following exposure to PQ for 72 h. When the cessation of the heartbeat and breathing of the rats was confirmed, and there were no reflexes, the death of the experimental animals was confirmed painlessly. Whole lung tissue was excised, dried and weighed. The left lung was placed in 10% paraformaldehyde and the right lung was placed in a cryopreservation tube and stored in a -80˚C refrigerator.

The experimental procedures were performed in accordance with the Guide for the Care and Use of Laboratory Animals and approved by the Ethics Committee of the First Affiliated Hospital of Hainan Medical University [approval no. 2020 (Research) No. (97); Haikou, China].

Haematoxylin and eosin (H&E) staining. Rat lung tissue were paraffin-embedded in paraffin after being fixed in 10% formaldehyde at room temperature for 24 h and cut into 4-μm-thick sections. After successful staining with haematoxylin and eosin, pathological changes were detected under a light microscope. Lung tissue damage was quantified using a score of 0 (normal) to 3 (severe) that included alveolar wall oedema, haemorrhage, vascular congestion and polymorphonuclear leukocyte infiltration. As previously reported, lung injuries were categorized according to the sum of the scores (27). Lung injuries were graded on a scale of severity from 0 to 5 (0, normal; 1, mild or very small amount; 2, mild or small amount; 3, moderate or larger amount; 4, severe or large amount; and 5, very severe or extremely large amount).

Evans blue staining. To determine pulmonary vascular permeability, Evans blue solution (2 mg/kg) was injected into the tail vein of rats, and the rats were euthanized 1 h after the injection. Lung tissue was perfused with PBS until the lungs turned white, resected as a whole, dried and weighed, and the right lung was weighed in half. The lung tissue was homogenized with formamide and incubated at 60˚C in a water bath protected from light for 24 h. After incubation, the suspension was centrifuged (4˚C, 13,400 x g, 15 min) and 200 μl of the supernatant was added to a 96-well plate, and the absorbance at 620 nm was measured using an enzyme counter. The amount of Evans blue dye was calculated using the standard curve method.

Immunohistochemical staining. Immunohistochemical staining was used to detect the protein expression of vascular endothelial-cadherin (VE-cadherin), zonula occludens-1 (ZO-1) and CD31 in paraffin sections (4-μm-thick) of lung tissues. Paraffin sections were dewaxed (environmental-friendly dewaxing solution; cat. no. G1128; Wuhan Servicebio Technology Co., Ltd.), rehydrated using descending alcohol series for antigen repair and recovered; and the sections were placed in 3% BSA (cat. no. 36100ES25; Shanghai Yeasen Biotechnology Co., Ltd.) for 30 min at room temperature for blocking, and then incubated overnight at 4˚C with VE-cadherin antibody (dilution, 1:50; cat. no. XF354429; Invitrogen; Thermo Fisher Scientific, Inc.), ZO-1 antibody (dilution, 1:1,000; cat. no. 21773-1-AP; Proteintech Group, Inc.) and CD31 antibody (dilution, 1:1,000; cat. no. GB113151; Wuhan Servicebio Technology Co., Ltd.), followed by incubation with HRP-labelled goat anti-rabbit IgG secondary antibody (dilution, 1:200; cat. no. GB23303; Wuhan Servicebio Technology Co., Ltd.) for 1 h at room temperature. Finally, the sections were stained with diaminobenzidine and counterstained with haematoxylin (room temperature, 3 min), and observed under a light microscope. Microscopic images were evaluated using ImageJ software (Fiji distribution of ImageJ; https://imagej.net/software/fiji/), and the area of VE-cadherin, ZO-1 and CD31-positive cells was quantified.

Cell culture and treatment. HPMECs were purchased from Otwo Biotechnology Development Co., Ltd. (cat. no. HTX2255) and cultured in DMEM (Gibco; Thermo Fisher Scientific, Inc.) containing 10% fetal bovine serum (Procell Life Science & Technology Co., Ltd.) with 5% CO_2 at 37˚C for proliferation. Cells were incubated with different concentrations of PQ pure (AccuStandard, Inc.) for 24, 48 and 72 h. The results are shown in Fig. S1A. Cell viability was reduced in a dose-dependent manner, and the reduction in cell viability was more pronounced after 72 h of treatment than at 48 and 24 h. Although the IC_{50} results ranged between 200 and 300 μM (Fig. 1C), the viability of the cells was <50% after 300 μM treatment. Therefore, a PQ dose of 200 μM was chosen for subsequent experiments to treat the cells for 72 h. HPMECs were then pre-treated with different concentrations of AH_2QDS for 2, 6 and 12 h, and 200 μM AH_2QDS had the least effect on cell viability (Fig. 2A and B). Therefore, 200 μM was selected as the concentration of AH_2QDS for subsequent experiments.

The cells were divided into the following four groups: Control group, HPMECs were treated with medium for 72 h; PQ group, cells were stimulated with PQ (200 μM) alone for 72 h; PQ + AH_2QDS group, HPMECs were treated with AH_2QDS (200 μM) for 2 h followed by stimulation of the cells with PQ (200 μM) for 72 h; and AH_2QDS group, cells were stimulated with AH_2QDS (200 μM) alone for 72 h.

Transwell cell migration assay. Experiments were performed using Transwell plates with a pore size of 5 μm to assess cell migration. Briefly, $3x10^4$ HPMECs were inoculated into the upper part of the migration chamber containing serum-free medium. The lower chamber was filled with complete medium containing 20% fetal bovine serum as an attractant. After 72 h of incubation, migratory cells were stained with 0.1% crystal violet (Biosharp Life Sciences) at room temperature for 10 min and non-migratory cells in the upper chamber were removed with a cotton swab. Cells were then imaged and counted under a light microscope.

Cell viability assay. To assess PQ and AH_2QDS cytotoxicity, HPMECs in the logarithmic growth phase were homogeneously inoculated into 96-well plates at a density of $3\text{-}5x10^3$ per cell culture (100 μl/well). After waiting for 12 h of cell apposition, the cells were treated with different concentrations of PQ for 24, 48 and 72 h. The cells were pre-treated with different concentrations of AH_2QDS for 2 h, and then treated with 200 μM PQ for 72 h. Cell Counting Kit-8 (CCK-8) solution

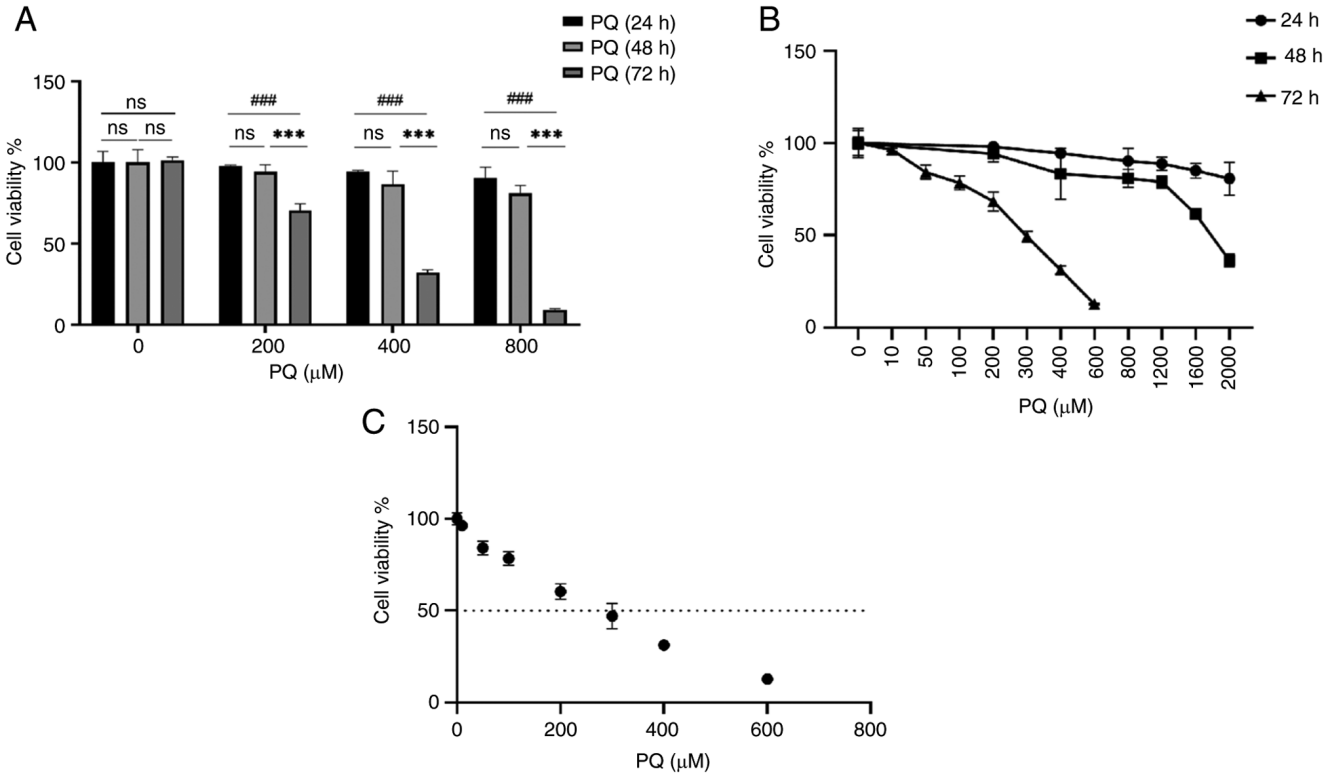

Figure 1. PQ induces dose- and time-dependent cytotoxicity in human pulmonary microvascular endothelial cells. (A) Cell viability was assessed after treating cells with 200, 400 and 800 μM for 24, 48 and 72 h. Data are expressed as the mean ± SEM of three independent experiments. Compared with the PQ (24 h) group, $^{###}$P<0.001. Compared with the PQ (48 h) group, ***P<0.001. The horizontal coordinate is concentration and the vertical coordinate is cell viability. (B) Line graph of cell viability after intervention of cells with PQ concentration gradient and time gradient. The horizontal coordinate is concentration and the vertical coordinate is cell viability. (C) IC_{50} for PQ concentrations. Data are expressed as the mean ± SEM of three independent experiments. PQ, paraquat; ns, not significant.

(10 μl) was added to each well according to the manufacturer's instructions (cat. no. BS350C; Anhui Biosharp Technology Co., Ltd.). The 96-well plates were further incubated in a 37˚C cell incubator for 1-2 h. Absorbance was measured at 450 nm using an enzyme marker.

Measurement of intracellular NO levels. Intracellular NO levels were measured using the fluorescent indicator diaminofluorescein-FM diacetate (DAF-FM DA; Shanghai Yeasen Biotechnology Co., Ltd.). Cells were inoculated at a density of $1x10^4$ per dish and cultured in confocal dishes, and cells were pre-treated with AH_2QDS for 2 h and stimulated with PQ (200 μM) for 72 h. After treatment, the medium was discarded and the cells were gently washed three times with PBS, and then the cells were treated with 200 μl DAF-FM DA (5 μM) for 30 min in a 37˚C cell incubator. Cells were washed three times using PBS and kept in PBS throughout the experiment. Finally, the fluorescence intensity was measured using a laser confocal microscope with an excitation wavelength of 488 nm and an emission wavelength of 515 nm. The measured fluorescence values were analysed using ImageJ software to examine the changes in fluorescence intensity in each group.

Detection of intracellular reactive oxygen species (ROS) levels. The level of intracellular ROS was measured using the Reactive Oxygen Detection kit (cat. no. BL714A; Anhui Biosharp Technology Co., Ltd.). Cells were inoculated at a density of $1x10^4$ per dish and cultured in confocal dishes, and cells were pre-treated with AH_2QDS for 2 h and stimulated with PQ (200 μM) for 72 h. After treatment, the medium was discarded and the cells were gently washed three times with PBS. Subsequently, the cells were treated with 200 μl 2',7'-dichlorodihydrofluorescein diacetate (10 μM) for 30 min at 37˚C in a cell culture incubator, and washed three times with PBS, and after that, the whole experiment was kept in serum-free medium. Finally, the fluorescence intensity was measured using a laser confocal microscope with an excitation wavelength of 488 nm and an emission wavelength of 515 nm. The measured fluorescence values were analysed using ImageJ software to examine the changes in fluorescence intensity in each group.

Detection of intracellular malondialdehyde (MDA) and superoxide dismutase (SOD) levels. After establishing the cell model, the cells were lysed with RIPA lysis solution and centrifuged at 13,400 g at 4˚C for 10 min, and the supernatant was the desired sample. According to the instructions of the MDA (cat. no. BL1481A; Anhui Biosharp Technology Co., Ltd.) and SOD (cat. no. A001-3-2; Nanjing Jiancheng Bioengineering Institute) detection kits, the relevant reagents were added to the reaction, and finally the absorbance values were measured using an enzyme marker at 532 and 450 nm, respectively.

ELISA. TNF-α, IL-1β and IL-6 levels in the supernatants of HPMECs were detected using a human ELISA kit (Fine Biotech Co., Ltd.) according to the manufacturer's instructions.

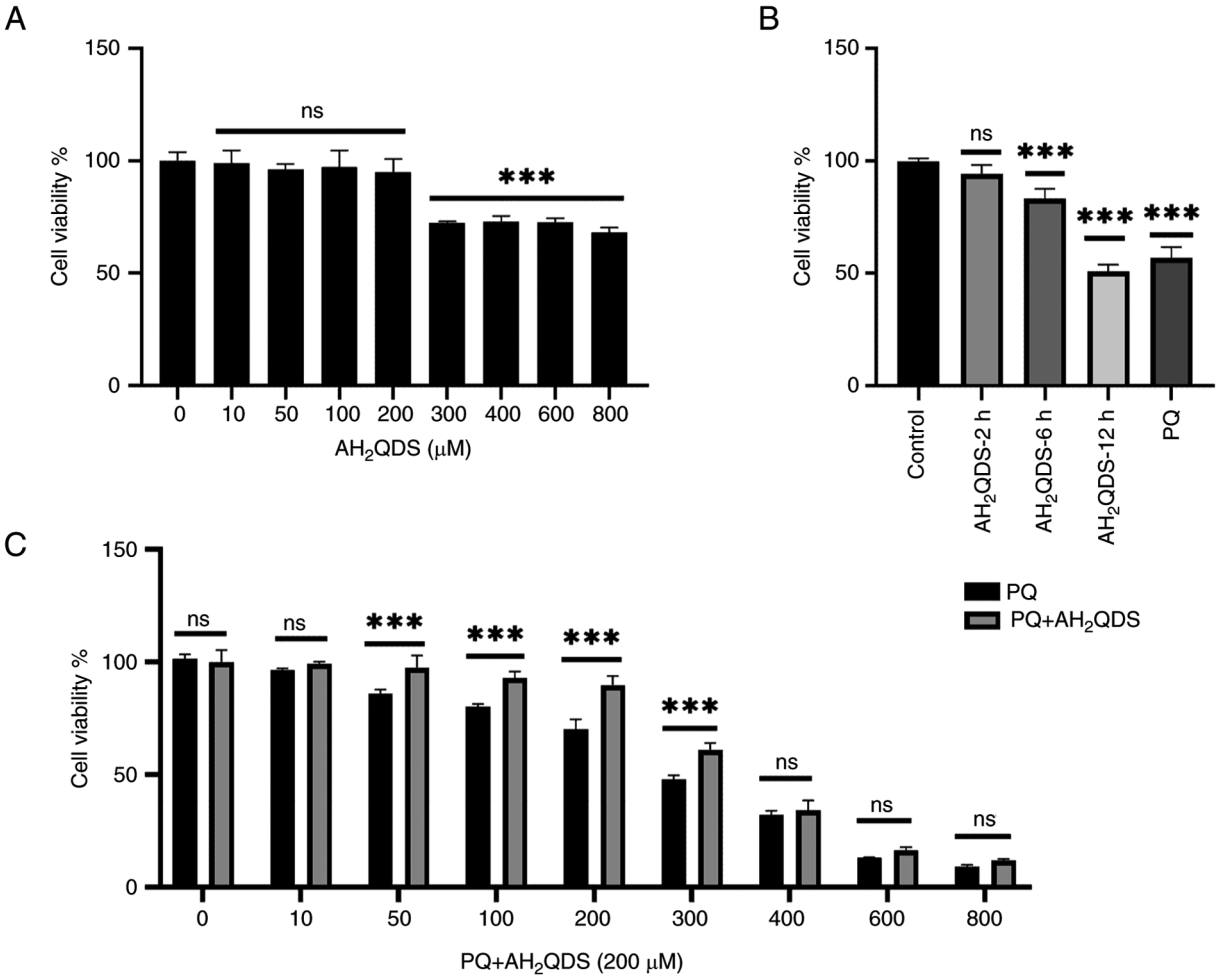

Figure 2. AH_2QDS attenuates PQ-induced cytotoxicity. (A) Cell viability was assessed after treating cells with 0, 10, 50, 100, 200, 300, 400, 600 and 800 μM AH_2QDS for 2 h. (B) Cell viability was assessed after treating the cells with 200 μM AH2QDS for 2, 6 and 12 h. (C) Cell viability was assessed after pretreatment with 200 μM for 2 h followed by treatment of cells with 0, 10, 50, 100, 200, 300, 400, 600, and 800 μM for 72 h. Data are expressed as the mean ± SEM of three independent experiments. Compared with the control (0 μM PQ), ***P<0.001. AH_2QDS, anthrahydroquinone-2,6-disulfonate; PQ, paraquat; not significant.

Western blotting (WB). The rat lung tissues and HPMECs were lysed with RIPA lysis buffer (cat. no. G2002-100ML; Wuhan Servicebio Technology Co., Ltd.) containing protease inhibitors (cat. no. BL612A; Anhui Biosharp Technology Co., Ltd.) to prepare protein samples. After quantification of the protein concentration using a BCA Protein Assay Kit (cat. no. 20201ES76; Shanghai Yeasen Biotechnology Co., Ltd.), protein samples (40 μg) were separated by 7.5-10% SDS-PAGE, and then transferred to PVDF transfer membranes. The membranes were blocked with 5% skimmed milk powder for 1 h at room temperature, and incubated with primary antibody at 4˚C overnight. The following primary antibodies were used: VE-cadherin antibody (dilution, 1:250; cat. no. XF354429; Invitrogen; Thermo Fisher Scientific, Inc.), ZO-1 antibody (dilution, 1:10,000; cat. no. 21773-1-AP; Proteintech Group, Inc.), IL-6 antibody (dilution, 1:1,500; cat. no. bs-0782R; BIOSS), IL-1β antibody (dilution, 1:1,000; cat. no. bs-0812R; BIOSS), TNF-α antibody (dilution, 1:1,000; cat. no. BP4903; Wuhan Boster Biological Technology, Ltd.), PI3K antibody (dilution, 1:1,000; cat. no. 20584-1-AP; Proteintech Group, Inc.), phosphorylated (p-)PI3K antibody (dilution, 1:1,000; cat. no. PA5-104853; Invitrogen; Thermo Fisher Scientific, Inc.), AKT antibody (dilution, 1:1,000; cat. no. 10176-2-AP; Proteintech Group, Inc.), p-AKT antibody (dilution, 1:1,000; cat. no. 28731-1-AP; Proteintech Group, Inc.), eNOS antibody (dilution, 1:1,000; cat. no. 27120-1-AP; Proteintech Group, Inc.), β-actin antibody (dilution, 1:1,000; cat. no. GB11001-100; Wuhan Servicebio Technology Co., Ltd.) and GAPDH antibody (dilution, 1:1,000; cat. no. GB15004-100; Wuhan Servicebio Technology Co., Ltd.). The membranes were washed at least three times with TBS with 1% Tween-20 (TBST) and incubated with secondary antibody conjugated to HRP-labelled goat anti-rabbit IgG (dilution, 1:10,000; cat. no. BL003A; Anhui Biosharp Technology Co., Ltd.) at room temperature for 2 h. After three washes with TBST, images of the bands were captured (Super ECL Detection Reagent-ECL Ultra-Sensitive Chemiluminescent Detection Kit; cat. no. 36208ES60; Shanghai Yeasen Biotechnology Co., Ltd.) and analysed using a chemical gel imager (CHAMP CHEMI TOP 610 PLUS).

Statistical analysis. All data are presented as the mean ± standard error of the mean (SEM) of at least three independent experiments and were analysed using GraphPad Prism8 software (Dotmatics). One-way ANOVA followed by Tukey's multiple comparison test was used to determine

differences between groups. P<0.05 was considered to indicate a statistically significant difference.

Results

PQ induces cytotoxicity in HPMECs. To study the cytotoxicity of PQ, cell viability was examined using a CCK-8 assay. Cells were treated with pure PQ (0, 200, 400, 800, 1,200, 1,600 and 2,000 μM) for 24 and 48 h, and cell viability was assessed at the end of culture. As shown in Fig. S1A and B, the inhibition of cell viability by PQ was dose- and time-dependent. After 24 h of PQ treatment, the cell viability was decreased following 1,600 μM PQ treatment (Fig. S1A), and after 48 h of PQ treatment, the cell viability was decreased following 1,200 μM PQ treatment, with a cell viability of >60% compared with the control in all cases (Fig. S1B). However, after 72 h of PQ treatment, the cell viability was significantly decreased following 200 μM PQ treatment, down to 59% compared with the control (Fig. S1C). When calculating the IC_{50} of PQ, the IC_{50} of PQ was 200-300 μM; however, at 300 μM, cell viability was <50%. Therefore, 200 μM was selected as the concentration of PQ for subsequent experiments (Fig. 1C). These results indicated that PQ induced cytotoxicity in HPMECs in a dose- and time-dependent manner (Fig. 1A and B).

AH_2QDS attenuates PQ-induced cytotoxicity in HPMECs. To investigate the effect of AH_2QDS on the proliferation of cells, cell viability was determined using the CCK-8 assay. Cells were treated with 0, 10, 50, 100, 200, 300, 400, 600 and 800 μM AH_2QDS for 24 h. Cell viability was assessed at the end of the incubation. As demonstrated in Fig. 2A, after 2 h, 0, 10, 50, 100 and 200 μM AH_2QDS treatment had no significant effect on cell viability (Fig. 2A); however, 300 μM AH_2QDS and other concentrations of AH_2QDS had an effect on cell viability. Furthermore, when treating the cells with 200 μM AH_2QDS for 2, 6 and 12 h, cell viability was decreased after 6 h of treatment (Fig. 2B), which demonstrated the time- and dose-dependent effects of AH_2QDS on the viability of HPMEVCs. To assess the protective effect of AH_2QDS against PQ-induced cytotoxicity, cells were pre-treated with 200 μM AH_2QDS for 2 h, and then cell viability was assessed after exposure to 200 μM PQ for 72 h. As revealed in Fig. 2C, pretreatment with AH_2QDS significantly increased the PQ-induced decrease in cell viability (Fig. 2C), but this protective effect was markedly reduced by PQ at concentrations >300 μM.

AH_2QDS inhibits the PQ-induced increase in oxidative stress and NO production in HPMECs. The intracellular oxidative stress level was assessed by detecting ROS, NO fluorescence intensity, MDA and SOD levels. As shown in Fig. 3A-D, the fluorescence intensity of ROS and NO in PQ-induced HPMECs was significantly higher compared with that in the control group, whereas the fluorescence intensity of ROS and NO in PQ-induced cells was decreased by pretreatment with AH_2QDS, suggesting that AH_2QDS could attenuate the production of ROS and NO in PQ-induced cells, thus reducing endothelial cell damage. As demonstrated in Fig. 3E and F, the levels of SOD and MDA were also examined in HPMECs. MDA levels were significantly higher and SOD levels were lower in the PQ group compared with the control group; while MDA levels were decreased and SOD levels were significantly higher in the PQ-induced cells after pretreatment with AH_2QDS, which indicated that AH_2QDS could attenuate the level of oxidative stress in the PQ-induced cells. As revealed in Fig. 3G-I, ELISA results revealed that AH_2QDS significantly inhibited the expression of TNF-α, IL-6 and IL-1β in PQ-induced HPMECs.

AH_2QDS promotes the migration of HPMECs and maintains normal cellular connectivity. The migration of HPMECs was detected using a Transwell assay. As displayed in Fig. 4A and B, the number of migratory cells in the PQ group was significantly lower compared with that in the control group, while the number was significantly higher after AH_2QDS treatment, which indicated that AH_2QDS could promote the migration of HPMECs. The intracellular protein expression levels of VE-cadherin and ZO-1 were detected by WB, and the results are shown in Fig. 4C-E. The protein expression levels of VE-cadherin and ZO-1 in the PQ group were significantly reduced, and the protein expression levels were significantly increased after AH_2QDS treatment, which demonstrated that AH_2QDS could maintain the normal connectivity of HPMECs. The fluorescence intensity of ZO-1 protein was detected using an immunofluorescence assay. The results in Fig. 4F and G indicated that ZO-1 protein expression was significantly reduced in the PQ group compared with the control group, and some cells were deficient in protein expression. This result was reversed by AH_2QDS treatment.

AH_2QDS treatment attenuates PQ-induced ALI in rats. To assess the effect of AH_2QDS on PQ-induced ALI in rats, a PQ-induced ALI rat model was constructed, and pathological changes in lung tissues were detected by H&E staining. As demonstrated in Fig. 5A, PQ treatment resulted in marked inflammatory infiltrates, destruction of alveolar and alveolar wall capillary structures, and pulmonary oedema in the lung tissues. These symptoms were markedly improved by AH_2QDS treatment. Additionally, as shown in Fig. 5B, the lung injury score was significantly higher in the PQ group compared with the control group, whereas the lung injury score was reduced after AH_2QDS treatment. To verify that AH_2QDS could reduce inflammation in lung tissues, the protein expression levels of IL-6, IL-1β and TNF-α in lung tissues were detected using WB. As indicated in Fig. 5C-F, the protein expression levels of IL-6, IL-1β and TNF-α in the PQ group were significantly increased compared with those in the control group; however, the protein expression levels of IL-6, IL-1β and TNF-α were significantly decreased after AH_2QDS treatment.

AH_2QDS improves PQ-induced pulmonary vascular permeability and connexin expression in rats. To verify that AH_2QDS reduces pulmonary oedema by decreasing pulmonary microvessel permeability and decreasing exudation, pulmonary microvessel permeability was examined using the Evans blue assay (Fig. 6A and B). The protein expression levels of VE-cadherin and ZO-1 in lung tissues were detected by WB, and the results were consistent with the results obtained in HPMECs (Fig. 6C-E). Immunohistochemical staining results

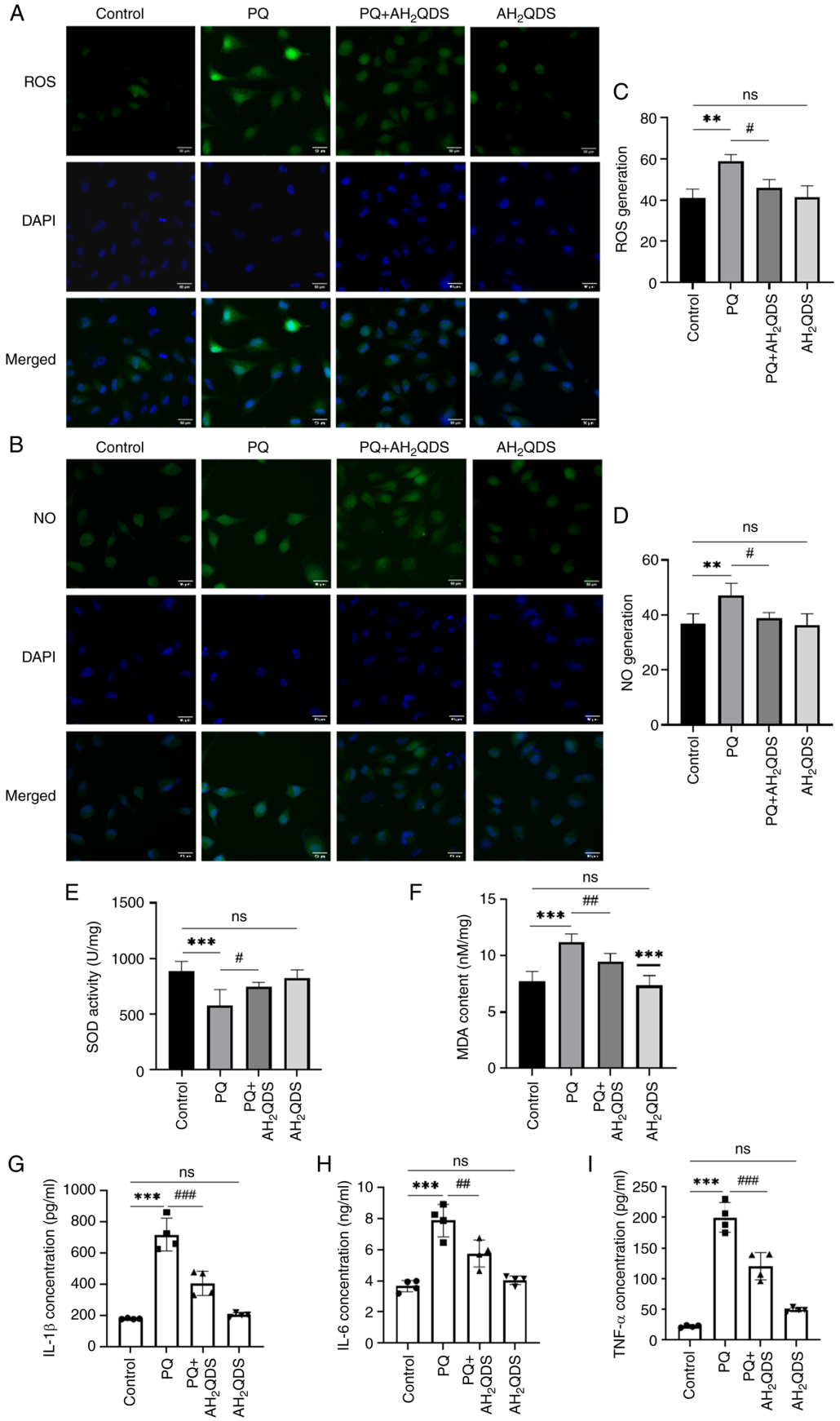

Figure 3. Effect of AH_2QDS on PQ-induced cellular oxidative stress and NO production. (A) ROS fluorescence detection of ROS content in cells in each group. Scale bar, 50 μm. ROS: green, DAPI: blue. (B) NO fluorescence detection of NO content in cells in each group. Scale bar, 50 μm. NO: green, DAPI: blue. (C and D) Quantitative analysis of ROS and NO in each group. (E and F) SOD and MDA content in each group of human pulmonary microvascular endothelial cells. (G-I) ELISA was performed to detect the expression levels of TNF-α, IL-6 and IL-1β in each group. Data are expressed as the mean ± SEM of three independent experiments. Compared with the control group, $^{**}P<0.01$ and $^{***}P<0.001$. Compared with the PQ group, $^{\#}P<0.05$, $^{\#\#}P<0.01$ and $^{\#\#\#}P<0.001$. AH_2QDS, anthrahydroquinone-2,6-disulfonate; PQ, paraquat; NO, nitric oxide; ROS, reactive oxygen species; SOD, superoxide dismutase; MDA, malondialdehyde; ns, not significant.

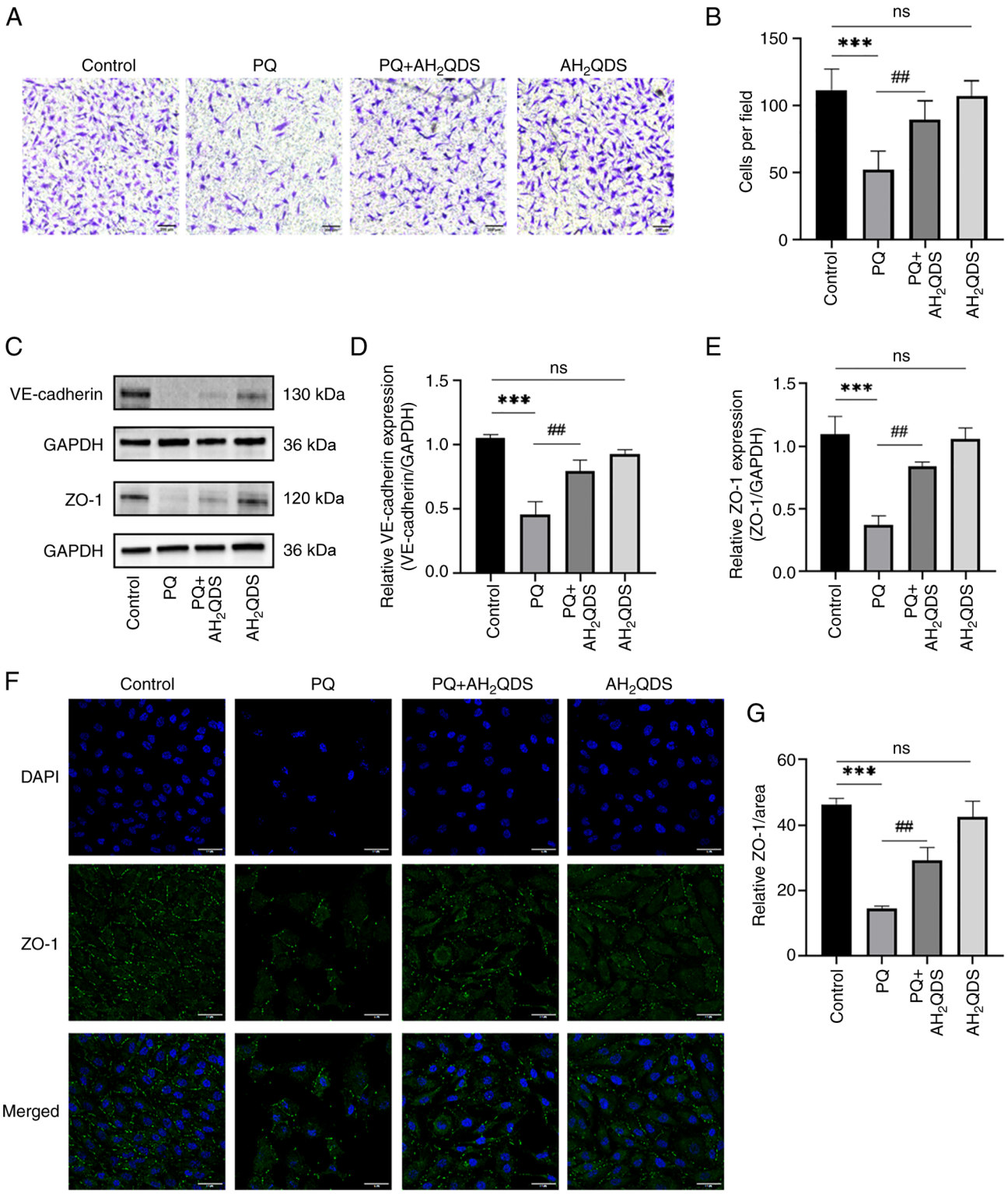

Figure 4. Effect of AH_2QDS on cell migration and connexin. (A) Transwell assay was used to detect that AH2QDS ameliorates the PQ-induced reduction in cell migration. Scale bar, 200 μm. (B) Number of migrating cells in the field of view. (C-E) VE-cadherin protein and ZO-1 protein levels in each group of HPMECs were detected by western blotting. (F) Expression of ZO-1 protein in each group of HPMECs was measured by confocal microscopy. Scale bar, 50 μm. ZO-1: green, DAPI: blue. (G) ZO-1 protein-positive area in each group. Data are expressed as the mean ± SEM of three independent experiments. Compared with the control group, ***P<0.001. Compared with the PQ group, $^{\#\#}$P<0.01. AH2QDS, anthrahydroquinone-2,6-disulfonate; PQ, paraquat; VE-cadherin, vascular endothelial-cadherin; ZO-1, zonula occludens-1; HPMECs, human pulmonary microvascular endothelial cells; ns, not significant.

showed that the protein expression levels of VE-cadherin, ZO-1 and CD31 were significantly reduced in lung tissues in rats; however, these were significantly increased in the AH_2QDS treatment group (Fig. 6F-I).

AH_2QDS ameliorates ALI by modulating the PI3K/AKT/eNOS signalling pathway. To further elucidate the underlying mechanisms of AH_2QDS for the management of PQ-induced endothelial dysfunction, the present study concentrated

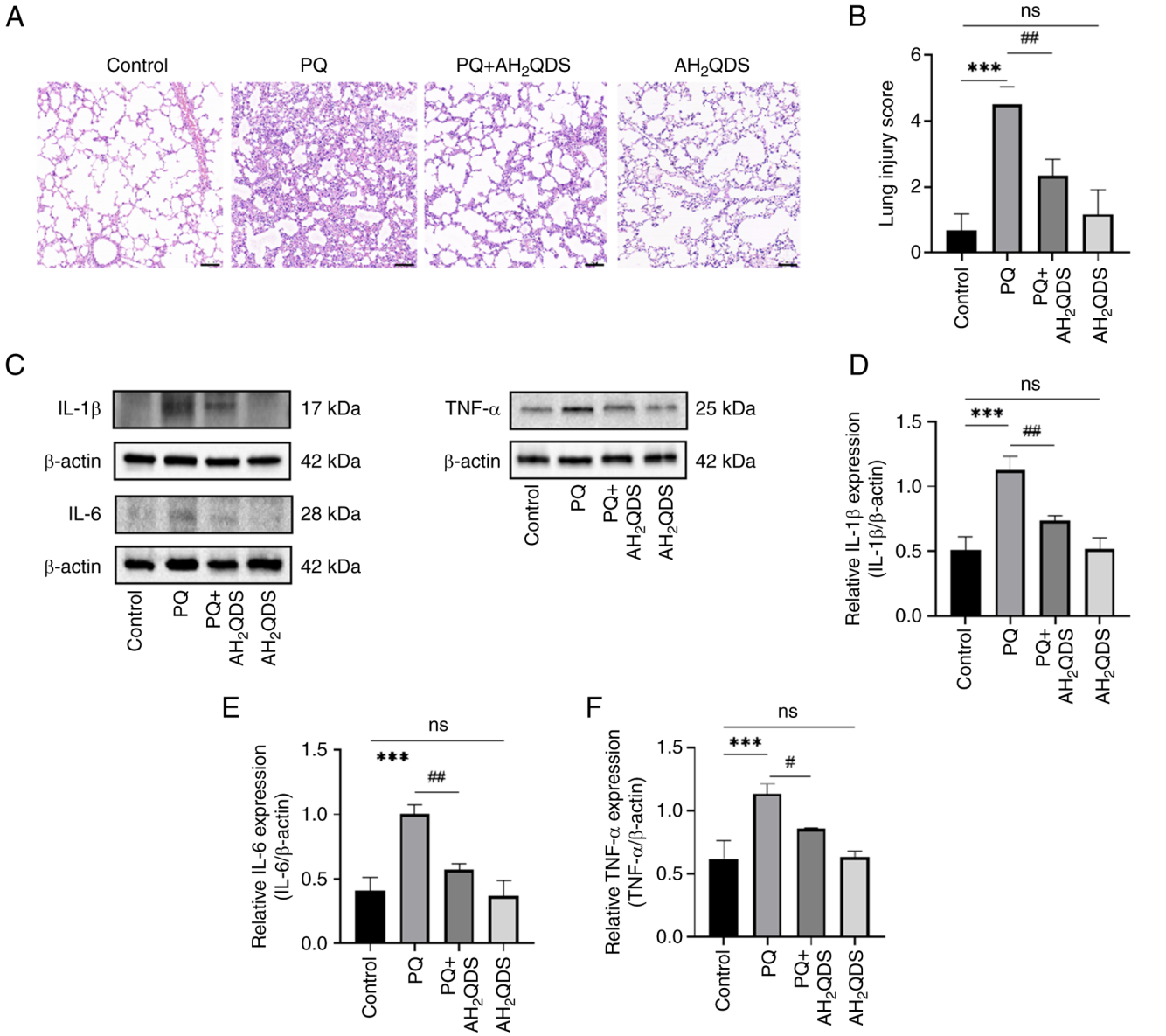

Figure 5. Effect of AH_2QDS on PQ-induced acute lung injury in SD rats. (A and B) H&E staining of lung tissue and scoring for assessment of lung injury. Scale bar, 100 μm. (C-F) Detection of IL-6, IL-1β and TNF-α protein levels in various groups of lung tissue by western blotting. Data are expressed as the mean ± SEM of three independent experiments. Compared with the control group, ***P<0.001. Compared with the PQ group, $^{\#}$P<0.05 and $^{\#\#}$P<0.01. AH_2QDS, anthrahydroquinone-2,6-disulfonate; PQ, paraquat; ns, not significant.

on the PI3K/AKT/eNOS signalling pathway. As shown in Fig. 7A-C, in rat lung tissues, p-PI3K and p-Akt protein levels were elevated in the PQ group compared with the control group, whereas AH_2QDS treatment reduced the protein levels of p-PI3K and p-Akt. As demonstrated in Fig. 7D and E, PQ increased eNOS expression in rat lung tissues, which was reversed to a certain extent by AH_2QDS treatment. As revealed in Fig. 7F-H, the protein levels of p-PI3K and p-Akt were elevated in HPMECs, whereas AH_2QDS treatment suppressed the protein levels of p-PI3K and p-Akt, which was consistent with the results of the *in vitro* model. The results demonstrated that the PI3K/AKT/eNOS signalling pathway was involved in the beneficial effect of AH_2QDS on PQ-induced ALI. The mechanism of AH_2QDS reducing PQ-induced pulmonary microvascular permeability is presented in Fig. 8.

Discussion

PQ-induced ALI/ARDS is an acute and life-threatening lung disease with a mortality rate of 50-70% (4). Studies have demonstrated that PQ is absorbed into the bloodstream and first contacts endothelial cells, leading to oxidative stress, the inflammatory response and increased vascular permeability in pulmonary vascular endothelial cells. This induces pulmonary oedema, intra-alveolar haemorrhage and inflammatory cell infiltration (10,20,28,29), leading to death in severe cases (30,31). The mechanism by which PQ leads to endothelial cell dysfunction has not been clarified clinically and there is a lack of specific drugs and therapeutic options. Therefore, improving the dysfunction of the alveolar microvascular barrier could delay the progression of ALI/ARDS, and thus, improve patient survival (19). A recent study by the authors

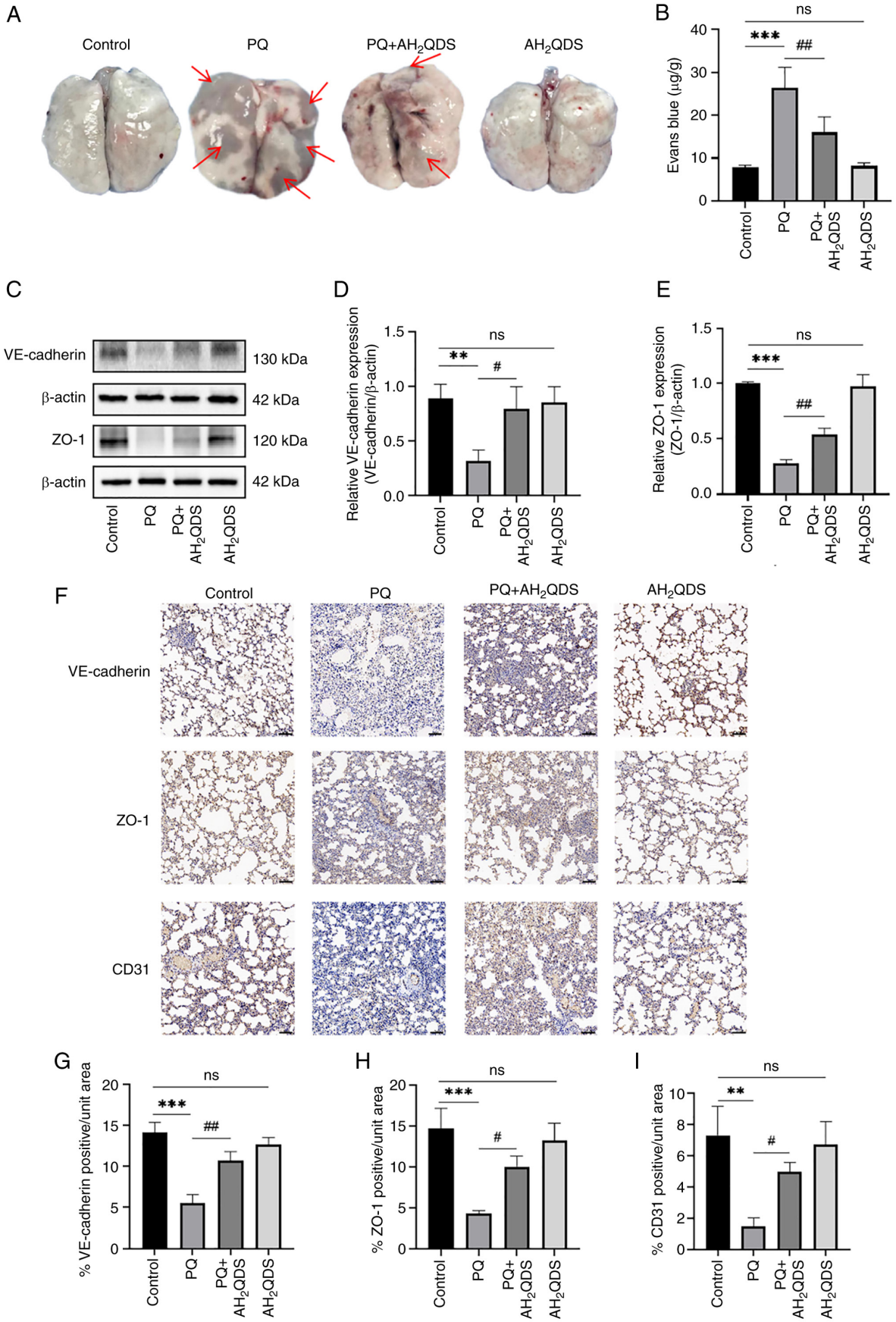

Figure 6. Effect of AH_2QDS on pulmonary microvascular permeability and connexin expression. (A and B) EB-stained lung tissue and content of EB lung tissue for determination of lung permeability in rats. Red arrows point to EB exudation. (C-E) Western blotting detection of VE-cadherin and ZO-1 protein levels in lung tissues of different groups of rats. (F) Immunohistochemical staining of VE-cadherin, ZO-1 and CD31 proteins in different groups. Scale bar, 100 μm. (G-I) Immunohistochemical analysis of VE-cadherin, ZO-1 and CD31 protein expression content in different groups of rat lung tissues. Data are expressed as the mean ± SEM of three independent experiments. Compared with the control group, **P<0.01 and ***P<0.001. Compared with the PQ group, $^{\#}$P<0.05 and $^{\#\#}$P<0.01. AH_2QDS, anthrahydroquinone-2,6-disulfonate; EB, Evans blue; ZO-1, zonula occludens-1; PQ, paraquat; ns, not significant.

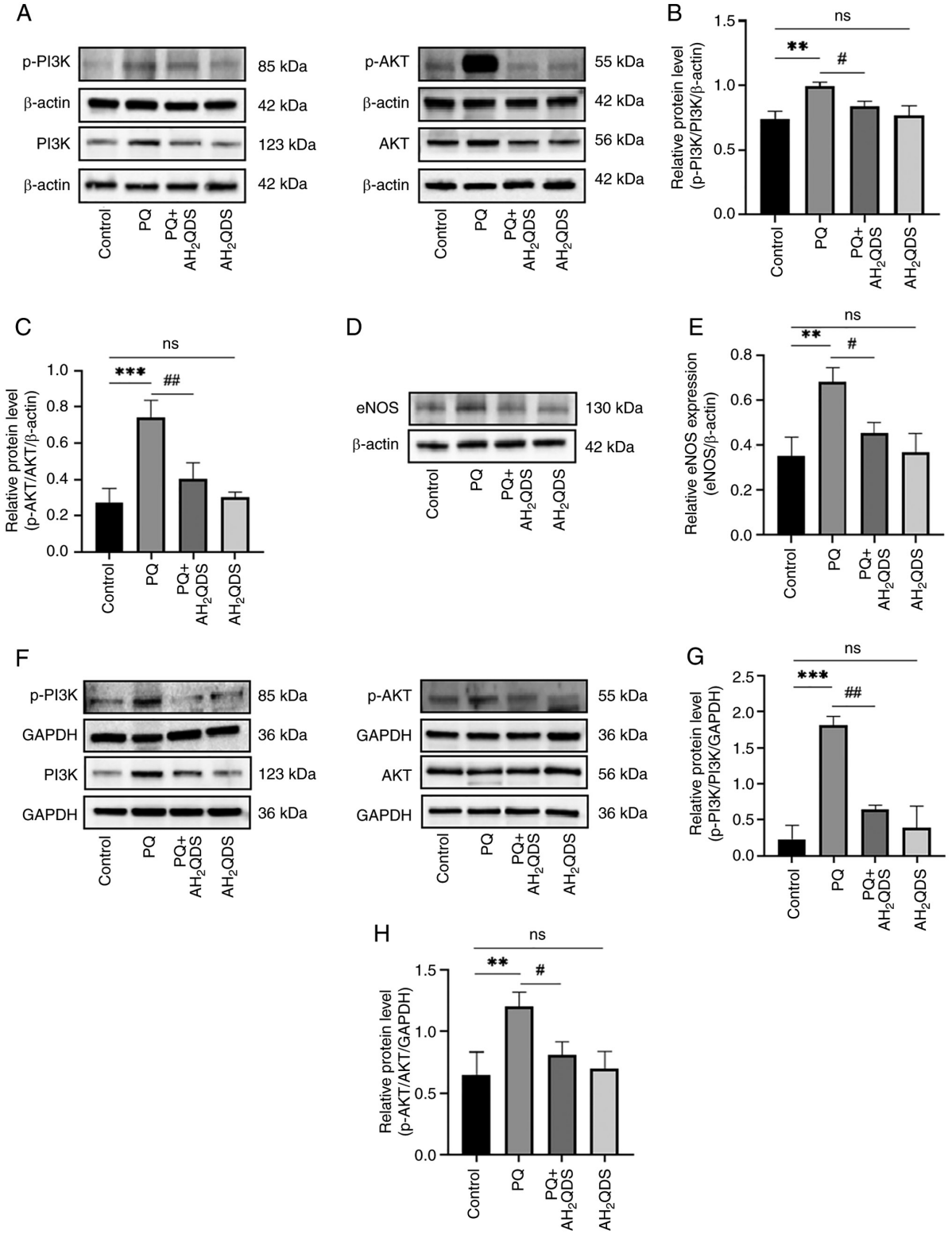

Figure 7. AH_2QDS ameliorates PQ-induced acute lung injury by modulating the PI3K/AKT/eNOS signalling pathway. (A-C) Expression levels of p-PI3K, PI3K, p-Akt and AKT proteins in different groups of lung tissues were detected by WB. (D and E) Expression levels of eNOS proteins in different groups of lung tissues detected by WB. (F-H) Expression levels of p-PI3K, PI3K, p-Akt and AKT proteins in different groups of human pulmonary microvascular endothelial cells were detected by WB. Data are expressed as the mean ± SEM of three independent experiments. Compared with the control group, $^{**}P<0.01$ and $^{***}P<0.001$. Compared with the PQ group, $^{\#}P<0.05$ and $^{\#\#}P<0.01$. AH_2QDS, anthrahydroquinone-2,6-disulfonate; PQ, paraquat; eNOS, eNOS, endothelial-type nitric oxide synthase; p-, phosphorylated; WB, western blotting; ns, not significant.

demonstrated that AH_2QDS could specifically bind to PQ to reduce the PQ concentration *in vivo* and improve survival in SD rats (20). AH_2QDS has both potent anti-inflammatory and antioxidant properties and is effective in the treatment of PQ-induced acute kidney injury. By constructing an *in vitro* model of PQ-induced ALI in SD rats and an *in vitro* model of

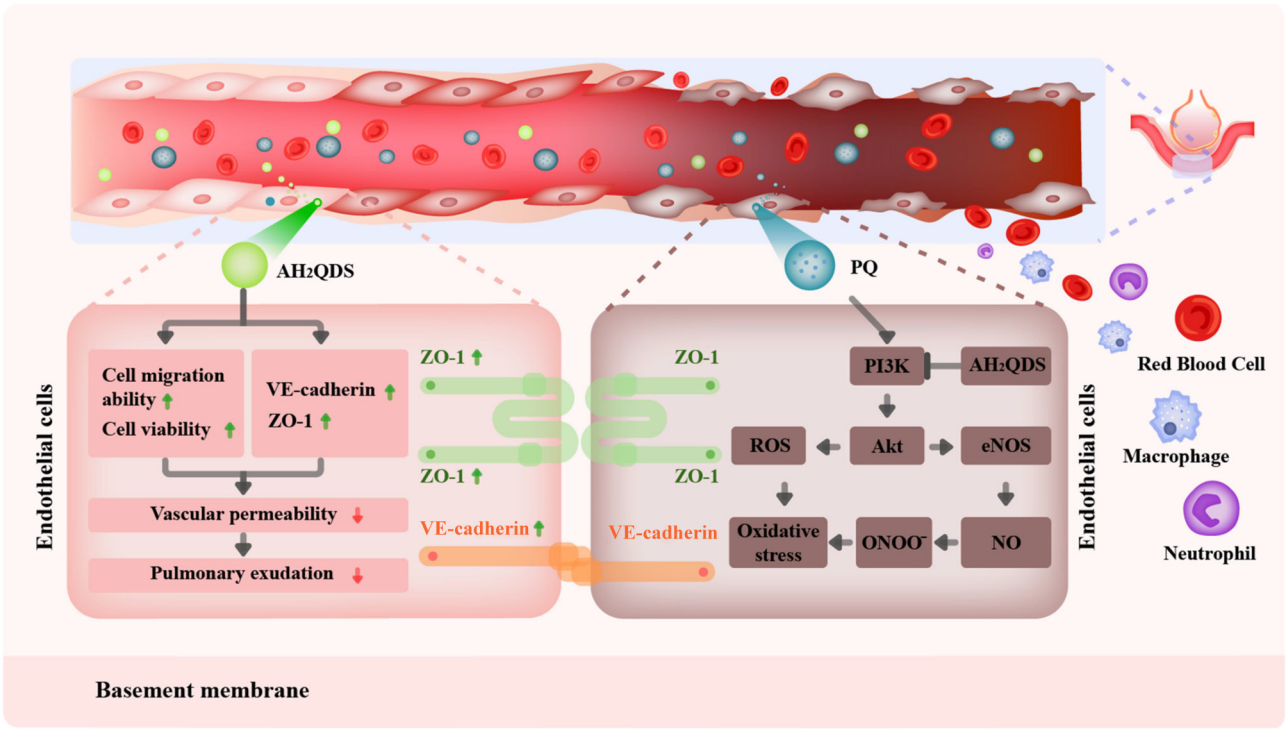

Figure 8. The mechanism of AH_2QDS reducing PQ-induced pulmonary microvascular permeability. AH2QDS, anthrahydroquinone-2,6-disulfonate; PQ, paraquat; ZO-1, zonula occludens-1.

PQ-induced endothelial dysfunction in HPMECs, the present study revealed that AH_2QDS has potential efficacy in treating PQ-induced endothelial cell dysfunction. AH_2QDS could attenuate PQ-induced ALI by inhibiting oxidative stress, inflammatory responses, promoting cell migration, enhancing cell viability and inhibiting the PI3K/AKT/eNOS signalling pathway to reduce pulmonary microvascular permeability.

Endothelial dysfunction is a major pathogenic mechanism in ALI/ARDS (12,32,33). The integrity of the endothelial barrier is disrupted after endothelial cells are damaged by multiple pathogenic factors. TJs, AJs and migration of endothelial cells maintain vascular permeability and reduce exudation and inflammatory infiltration. These functions maintain endothelial barrier function and integrity (34-36). In the present study, PQ-induced ALI tissues were markedly damaged with increased pulmonary microvascular permeability. This was manifested by pulmonary oedema, haemorrhage and inflammatory cell infiltration; lung injury assessment also verified that PQ-induced ALI induced excessive ROS production and inflammatory responses. VE-cadherin is the major TJ between endothelial cells. In ALI/ARDS, increased permeability following disruption of VE-cadherin and its adhesion complexes occurs with increased lung tissue leakage (37). ZO-1 is a key structure of AJs that directly affects lung barrier permeability. When ZO-1 expression is inhibited, lung permeability increases and lung barrier function is impaired (38). CD31 is a vascular endothelial cell-specific protein, and it has been similarly demonstrated that maintaining vascular integrity can effectively control the course of ALI/ARDS (39,40). The present study demonstrated that AH_2QDS attenuated the PQ-induced inflammatory response and oxidative stress in HPMECs, upregulated the decrease in VE-cadherin and ZO-1 protein expression due to PQ, reduced pulmonary microvascular permeability, and ameliorated pulmonary oedema. Elevated levels of pro-inflammatory mediators in the lungs of patients with ALI impair endothelial cell functions, including proliferation and migration (41,42). These toxic effects lead to an imbalance between vasodilation and constriction, accelerating endothelial dysfunction, disrupting vascular homeostasis, and leading to an increase in vascular permeability, which further exacerbates interstitial lung leakage. This is consistent with the present experimental results, which demonstrated that AH_2QDS could markedly improve endothelial cell migration, promote endothelial cell migration to the site of injury and maintain the integrity of the pulmonary microvasculature. These data suggested that AH_2QDS ameliorated PQ-induced ALI by improving endothelial dysfunction.

In the present experiments, it was found that during the pre-treatment of HPMECs with AH_2QDS, exceeding a certain concentration range can adversely affect the cell viability of HPMECs. Firstly, as a reducing agent, excessive use of AH_2QDS may disrupt the balance of intracellular redox reactions, and this imbalance could potentially damage the cell structure and function. Secondly, as a newly emerging drug, the stability of AH_2QDS and its mechanism of interaction with cells still require further exploration. Furthermore, different cell types may exhibit varying reactions to AH_2QDS, indicating that the impact of AH_2QDS on cell viability is a complex and multifaceted process. This discovery not only reveals the issues that need to be addressed in the application of AH_2QDS as a reducing agent, but also underscores its potential in scientific research. Further studies and verifications are needed to gain a deeper understanding of the mechanism of action of AH_2QDS, thereby providing new treatment strategies

and potential drug candidates for medical fields such as ALI related to PQ.

In a previous study by the authors, KEGG pathway enrichment analysis revealed that the PI3K/AKT signalling pathway was the main signalling pathway for gene enrichment in lung tissues after PQ poisoning and AH_2QDS treatment (26). The PI3K/AKT signalling pathway is important in the regulation of cell survival as well as repairing endothelial damage (43-47). To further investigate the mechanism by which AH_2QDS alleviated PQ-induced ALI, the present study focused on the PI3K/AKT/eNOS signalling pathway. eNOS is an enzyme present in large quantities that is expressed in several cell types and promotes the production of NO. During inflammation, eNOS induces large amounts of NO production, generating peroxynitrite anion, which causes damage to the vascular endothelium and contributes to the development of inflammation (48,49). eNOS serves as a downstream target of AKT, and the PI3K/AKT/eNOS signalling pathway is also an important signalling pathway in cells. The present study demonstrated that the expression levels of PI3K, AKT and eNOS were elevated in lung tissues after PQ intoxication, whereas the expression levels of PI3K, AKT and eNOS were significantly lower in lung tissues treated with AH_2QDS compared with the previous ones. The NO fluorescence intensity was significantly higher in HPMECs compared with the control group, and significantly decreased after AH_2QDS treatment compared with the PQ group. It was demonstrated that AH_2QDS could inhibit the PI3K/AKT/eNOS signalling pathway to attenuate the inflammatory response of endothelial cells. Therefore, the present study revealed that the mechanism by which AH_2QDS alleviated endothelial dysfunction during PQ-induced ALI progression was related to the PI3K/Akt/eNOS signalling pathway.

In recent years, organoid technology has become an indispensable model system in lung research. Besides being cultivated from adult lung stem/progenitor cells, lung organoids can also be derived from fetal tissue or induced pluripotent stem cells, greatly filling the technological gap in modelling lung development *in vitro* (50). With continuous technological advancements, significant progress has been made in the characterization and refinement of organoid culture systems (51). The strategic implementation and continuous improvement of this technology will provide exciting new opportunities for us to deeply understand and explore new treatment methods, potentially leading to significant improvements in the health conditions of patients with lung diseases. With the continuous progress of organoid technology, its application exploration in the field of lung diseases is increasingly deepening. This 3D spatial structure constructed by different types of epithelial cells, with its significant advantages of requiring a small number of samples and short construction time, has effectively compensated for the shortcomings of traditional 2D cell culture and animal models. Therefore, the organoid model has become an efficient *in vitro* model for lung disease research, drug screening and disease prediction, while also meeting strict ethical requirements for experiments. It is involved in multiple fields such as non-specific inflammation, infection and lung tumors. Especially during the period of the novel coronavirus infection (COVID-19), numerous researchers have actively attempted to use organoid technology to construct research models for COVID-19 to explore effective treatment options, thereby reducing respiratory symptoms, risks of multi-organ failure and mortality (52,53). Additionally, some studies have demonstrated the great potential of organoid technology. For instance, Okabe *et al* (54) found that orthotopic fetal lung tissue direct injection into the lungs of mice showed a preventive effect against PQ-induced ALI. Meanwhile, Chen *et al* (55) discovered that luteolin enhances trans-epithelial sodium transport in 3D alveolar epithelial organoid, effectively reducing respiratory symptoms. These studies have fully proven that organoid technology has broad application prospects in the field of personalized medicine.

In reviewing the current research, some limitations were indeed identified. Firstly, while the present study focused on the protective effect of AH_2QDS on PQ-induced lung microvascular endothelial dysfunction and its potential mechanism, it has not yet compared this finding with the latest progress in organoid research. As an emerging research tool, organoids have shown great potential in simulating human organ functions. Therefore, in future work, the authors will consider incorporating the application of AH_2QDS in organoid models into the research scope to further validate its effect and mechanism. Secondly, although the present study revealed the beneficial effects of AH_2QDS on lung tissue, it has not yet deeply identified the key genetic targets of its action. To fully understand the mechanism of AH_2QDS, high-throughput research such as proteomics will be conducted to find and validate the key genes and proteins related to the function of AH_2QDS. Additionally, the present study primarily focused on the protective effect of AH_2QDS on rat lung tissue, but it is unclear whether other organs can also benefit from it. To broaden the application range of AH_2QDS, its protective effects will be investigated on other organs (including the heart and brain) in subsequent studies and explore its potential mechanisms. In terms of signaling pathway research, while the present study paid attention to the importance of the PI3K/AKT signaling pathway in the action of AH_2QDS, it lacks direct experimental evidence of intervention in this pathway. Therefore, PI3K inhibitors and activators will be introduced in subsequent studies to clarify the specific role of the PI3K/AKT signaling pathway in the action of AH_2QDS. Finally, to more comprehensively evaluate the therapeutic effect of AH_2QDS, comparative studies with other types of inhibitors will be conducted. Finally, to more comprehensively evaluate the therapeutic effect of AH_2QDS in treating ALI, a series of comparative studies will be conducted. AH_2QDS shall be compared with traditional Chinese medicines such as Yu-Ping-Feng-San and Xuanfei Baidu Formula to explore their differences in improving ALI symptoms and reducing inflammatory responses. Additionally, AH_2QDS shall be also compared with emerging synthetic drugs, such as inhalable nanomaterials and extracellular vesicles, which have shown potential value in the treatment of ALI in recent years. Through these comparative studies, it is expected to gain a more comprehensive understanding of the advantages and limitations of AH_2QDS in treating ALI, providing a more scientific basis for future clinical applications. In summary, a series of follow-up studies will be conducted to improve the mechanism of action and therapeutic effect evaluation of AH_2QDS, aiming to provide new ideas and methods for the prevention and treatment of related diseases.

In conclusion, AH_2QDS attenuated PQ-induced ALI by inhibiting the PI3K/Akt/eNOS signalling pathway, suppressing inflammatory responses and oxidative stress, promoting cell proliferation and migration, and reducing pulmonary vascular hyperpermeability. These findings suggested that AH_2QDS may serve as an effective potential therapeutic agent for reversing ALI/ARDS outcomes caused by PQ.

Acknowledgements

Not applicable.

Funding

The present study was supported by the National Natural Science Foundation of China (grant no. 81960351) and the High-level Talent Fund of Hainan (grant no. 822RC835).

Availability of data and materials

The data generated in the present study may be requested from the corresponding author.

Authors' contributions

NL, YY and JC conceived and designed the study. YH, JP and ZL provided administrative support. All authors provided study materials. YW and JZ collected and assembled the data. CX and HL analyzed the data. NL and YY wrote the manuscript. NL and YY confirm the authenticity of all the raw data. JL and XL were responsible for the critical review of the manuscript. All authors participated in interpretation of the data. All authors read and approved the final manuscript.

Ethics approval and consent to participate

The present study was approved [approval no. 2020 (Research) No. (97)] by the Ethics Committee of the First Affiliated Hospital of Hainan Medical University (Haikou, China), and was carried out in accordance with the ethical standards of experimental animals.

Patient consent for publication

Not applicable.

Competing interests

The authors declare that they have no competing interests.

References

1. Zhang D, Shen F, Ma S, Nan S, Ma Y, Ren L, Li H and Yu Q: Andrographolide alleviates paraquat-induced acute lung injury by activating the Nrf2/HO-1 pathway. Iran J Basic Med Sci 26: 653-661, 2023.
2. Amin F, Memarzia A, Roohbakhsh A, Shakeri F and Boskabady MH: Zataria multiflora and pioglitazone affect systemic inflammation and oxidative stress induced by inhaled paraquat in rats. Mediators Inflamm 2021: 5575059, 2021.
3. Ying H, Kang Y, Zhang H, Zhao D, Xia J, Lu Z, Wang H, Xu F and Shi L: MiR-127 modulates macrophage polarization and promotes lung inflammation and injury by activating the JNK pathway. J Immunol 194: 1239-1251, 2015.
4. Zhang Y, Yuan D, Li Y, Yang F, Hou L, Yu Y, Sun C, Duan G, Meng C, Yan H, *et al*: Paraquat promotes acute lung injury in rats by regulating alveolar macrophage polarization through glycolysis. Ecotoxicol Environ Saf 223: 112571, 2021.
5. Li Y, Wang N, Ma Z, Wang Y, Yuan Y, Zhong Z, Hong Y and Zhao M: Lipoxin A4 protects against paraquat-induced acute lung injury by inhibiting the TLR4/MyD88-mediated activation of the NF-κB and PI3K/AKT pathways. Int J Mol Med 47: 86, 2021.
6. Li T, Cheng S, Xu L, Lin P and Shao M: Yue-bi-tang attenuates adriamycin-induced nephropathy edema through decreasing renal microvascular permeability via inhibition of the Cav-1/eNOS pathway. Front Pharmacol 14: 1138900, 2023.
7. Huang Y and He Q: Inhibition of c-Src protects paraquat induced microvascular endothelial injury by modulating caveolin-1 phosphorylation and caveolae mediated transcellular permeability. Environ Toxicol Pharmacol 52: 62-68, 2017.
8. Hu J, Chen R, An J, Wang Y, Liang M and Huang K: Dauricine attenuates vascular endothelial inflammation through inhibiting NF-κB pathway. Front Pharmacol 12: 758962, 2021.
9. Wu B, Xu MM, Fan C, Feng CL, Lu QK, Lu HM, Xiang CG, Bai F, Wang HY, Wu YW and Tang W: STING inhibitor ameliorates LPS-induced ALI by preventing vascular endothelial cells-mediated immune cells chemotaxis and adhesion. Acta Pharmacol Sin 43: 2055-2066, 2022.
10. Lin F, Yang Y, Wei S, Huang X, Peng Z, Ke X, Zeng Z and Song Y: Hydrogen sulfide protects against high glucose-induced human umbilical vein endothelial cell injury through activating PI3K/Akt/eNOS pathway. Drug Des Devel Ther 14: 621-633, 2020.
11. Wang RH, Xie YX, Qiu JW and Chen JY: Influence of LincRNA-p21 on acute lung injury in sepsis. Eur Rev Med Pharmacol Sci 24: 5618-5626, 2020.
12. Hao Y, Wang Z, Frimpong F and Chen X: Calcium-permeable channels and endothelial dysfunction in acute lung injury. Curr Issues Mol Biol 44: 2217-2229, 2022.
13. Duan Y, Learoyd J, Meliton AY, Leff AR and Zhu X: Inhibition of Pyk2 blocks lung inflammation and injury in a mouse model of acute lung injury. Respir Res 13: 4, 2012.
14. Pang L, Deng P, Liang YD, Qian JY, Wu LC, Yang LL, Yu ZP and Zhou Z: Lipoic acid antagonizes paraquat-induced vascular endothelial dysfunction by suppressing mitochondrial reactive oxidative stress. Toxicol Res (Camb) 8: 918-927, 2019.
15. Cong P, Tong C, Mao S, Shi L, Shi X, Liu Y, Jin H, Liu Y and Hou M: DDAH1 promotes lung endothelial barrier repair by decreasing leukocyte transendothelial migration and oxidative stress in explosion-induced lung injury. Oxid Med Cell Longev 2022: 8407635, 2022.
16. Wu C, Li F and Zhou S: Humus respiration and its ecological significance. Acta Ecol Sin 29: 1535-1542, 2009.
17. Chunyuan W, Qinfen L and Dongming W: A rapid detoxification solution and method for glyphosate. CN Patent 201610341330.6. Filed May 23, 2016; issued September 21, 2016.
18. Wu C, Wu D, Liu X, Qian J and Li Q: A specific antidote for acute paraquat poisoning. CN Patent 201910908879.2. Filed September 25, 2019; issued December 20, 2019.
19. Qian J, Wu CY, Wu DM, Li LH, Li Q, Deng T, Huang QF, Xu SQ, Wang HF, Wu XX, *et al*: Anthrahydroquinone-2-6-disulfonate is a novel, powerful antidote for paraquat poisoning. Sci Rep 11: 20159, 2021.
20. Li Q, Wang B, Lin KW, Deng T, Huang QF, Xu SQ, Wang HF, Wu XX, Li N, Yi Y, *et al*: Anthrahydroquinone-2,6-disulfonate alleviates paraquat-induced kidney injury via the apelin-APJ pathway in rats. Asian Pac J Trop Biomed 12: 333-342, 2022.
21. Ahmed MAE, El Morsy EM and Ahmed AAE: Protective effects of febuxostat against paraquat-induced lung toxicity in rats: Impact on RAGE/PI3K/Akt pathway and downstream inflammatory cascades. Life Sci 221: 56-64, 2019.
22. Luo W, Tao Y, Chen S, Luo H, Li X, Qu S, Chen K and Zeng C: Rosmarinic acid ameliorates pulmonary ischemia/reperfusion injury by activating the PI3K/Akt signaling pathway. Front Pharmacol 13: 860944, 2022.
23. Qi D, Tang X, He J, Wang D, Zhao Y, Deng W, Deng X, Zhou G, Xia J, Zhong X and Pu S: Omentin protects against LPS-induced ARDS through suppressing pulmonary inflammation and promoting endothelial barrier via an Akt/eNOS-dependent mechanism. Cell Death Dis 7: e2360, 2016.

24. Gopallawa I, Kuek LE, Adappa ND, Palmer JN and Lee RJ: Small-molecule Akt-activation in airway cells induces NO production and reduces IL-8 transcription through Nrf-2. Resp Res 22: 267, 2021.
25. Liu F, Sa Y , Li Y, Liu R, Wang Z, Li S, Zhang Y and Ma Z: Research progress on the correlation between acute hypoxic lung injury and NO, eNOS. Med Innov China 19: 184-188, 2022 (In Chinese).
26. Li N, Huang Y, Yi Y, Qian J, Li Q, Xu SQ, Wang HF, Wu XX, Peng JC, Li LH, *et al*: Analysis of abnormal expression of signaling pathways in PQ-induced acute lung injury in SD rats based on RNA-seq technology. Inhal Toxicol 36: 1-12, 2024.
27. Chen H, Li N, Zhan X, Zheng T, Huang X, Chen Q, Song Z, Yang F, Nie H, Zhang Y, *et al*: Capsaicin protects against lipopolysaccharide-induced acute lung injury through the HMGB1/NF-κB and PI3K/AKT/mTOR pathways. J Inflamm Res 14: 5291-5304, 2021.
28. Tatjana V, Domitille S and Jean-Charles S: Paraquat-induced cholesterol biosynthesis proteins dysregulation in human brain microvascular endothelial cells. Sci Rep 11: 18137, 2021.
29. Song CY, Feng MX, Li L, Wang P, Lu X and Lu YQ: Tripterygium wilfordii Hook.f. ameliorates paraquat-induced lung injury by reducing oxidative stress and ferroptosis via Nrf2/HO-1 pathway. Ecotoxicol Environ Saf 252: 114575, 2023.
30. Jiang J, Huang K, Xu S, Garcia JGN, Wang C and Cai H: Targeting NOX4 alleviates sepsis-induced acute lung injury via attenuation of redox-sensitive activation of CaMKII/ERK1/2/MLCK and endothelial cell barrier dysfunction. Redox Biol 36: 101638, 2020.
31. Cai Q, Jin Y, Jia Z and Liu Z: Paraquat induces lung injury via miR-199-mediated SET in a mouse model. Front Pharmacol 13: 856441, 2022.
32. Shen K, Wang X, Wang Y, Jia Y, Zhang Y, Wang K, Luo L, Cai W, Li J, Li S, *et al*: miR-125b-5p in adipose derived stem cells exosome alleviates pulmonary microvascular endothelial cells ferroptosis via Keap1/Nrf2/GPX4 in sepsis lung injury. Redox Biol 62: 102655, 2023.
33. Kim Y, Bae CR, Kim D, Kim H, Lee S, Zhang H, Noh M, Kim YM, Mochizuki N and Kwon YG: Efficacy of CU06-1004 via regulation of inflammation and endothelial permeability in LPS-induced acute lung injury. J Inflamm (Lond) 20: 13, 2023.
34. Komarova YA, Kruse K, Mehta D and Malik AB: Protein interactions at endothelial junctions and signaling mechanisms regulating endothelial permeability. Circ Res 120: 179-206, 2017.
35. Dong W, He B, Qian H, Liu Q, Wang D, Li J, Wei Z, Wang Z, Xu Z, Wu G, *et al*: RAB26-dependent autophagy protects adherens junctional integrity in acute lung injury. Autophagy 14: 1677-1692, 2018.
36. Meng XY, Lu QY, Zhang JF, Li JF, Shi MY, Huang SY, Yu SF, Zhao YM and Fan HJ: A novel animal model of primary blast lung injury and its pathological changes in mice. J Trauma Acute Care Surg 93: 530-537, 2022.
37. Xia W, Zhang H, Pan Z, Li G, Zhou Q, Hu D and Liu Y: Inhibition of MRP4 alleviates sepsis-induced acute lung injury in rats. Int Immunopharmacol 72: 211-217, 2019.
38. Zhou W, Shi G, Bai J, Ma S, Liu Q and Ma X: Colquhounia root tablet protects rat pulmonary microvascular endothelial cells against TNF-α-induced injury by upregulating the expression of tight junction proteins claudin-5 and ZO-1. Evid Based Complement Alternat Med 2018: 1024634, 2018.
39. Birnhuber A, Fließer E, Gorkiewicz G, Zacharias M, Seeliger B, David S, Welte T, Schmidt J, Olschewski H, Wygrecka M and Kwapiszewska G: Between inflammation and thrombosis: Endothelial cells in COVID-19. Eur Respir J 58: 2100377, 2021.
40. Zhao Y, Jin H, Lei K, Bai LP, Pan H, Wang C, Zhu X, Tang Y, Guo Z, Cai J and Li T: Oridonin inhibits inflammation of epithelial cells via dual-targeting of CD31 Keap1 to ameliorate acute lung injury. Front Immunol 14: 1163397, 2023.
41. Yang N, Tian H, Zhan E, Zhai L, Jiao P, Yao S, Lu G, Mu Q, Wang J, Zhao A, *et al*: Reverse-D-4F improves endothelial progenitor cell function and attenuates LPS-induced acute lung injury. Respir Res 20: 131, 2019.
42. Chen DQ, Shen MJ, Wang H, Li Y, Tang AL, Li S, Xiong MC, Guo Y and Zhang GQ: Sirt3 maintains microvascular endothelial adherens junction integrity to alleviate sepsis-induced lung inflammation by modulating the interaction of VE-cadherin and β-catenin. Oxid Med Cell Longev 2021: 8978795, 2021.
43. Singh D, Kumar V and Singh C: IFN-γ regulates xanthine oxidase-mediated iNOS-independent oxidative stress in maneb- and paraquat-treated rat polymorphonuclear leukocytes. Mol Cell Biochem 427: 133-143, 2017.
44. Li N, Sun W, Zhou X, Gong H, Chen Y, Chen D and Xiang F: Dihydroartemisinin protects against dextran sulfate sodium-induced colitis in mice through inhibiting the PI3K/AKT and NF-κB signaling pathways. Biomed Res Int 2019: 1415809, 2019.
45. Wang L, Tang X and Li S: Propofol promotes migration, alleviates inflammation, and apoptosis of lipopolysaccharide-induced human pulmonary microvascular endothelial cells by activating PI3K/AKT signaling pathway via upregulating APOM expression. Drug Dev Res 83: 397-406, 2022.
46. Li YH, Yuan Y, Wang YW and Zhao M: The role of PI3K/AKT-mediated apoptosis signaling pathway in paraquat poisoning-induced cardiac injury. Chin J Diffic Compl Cas 20: 278-282, 2021.
47. Zhong R, Xia T, Wang Y, Ding Z, Li W, Chen Y, Peng M, Li C, Zhang H and Shu Z: Physalin B ameliorates inflammatory responses in lipopolysaccharide-induced acute lung injury mice by inhibiting NF-κB and NLRP3 via the activation of the PI3K/Akt pathway. J Ethnopharmacol 284: 114777, 2022.
48. Xin W, Yanxia Z, Haixia L, Aijun L, Shuang L, Huimin C and Zheng CW: Effect of i NOS and cell apoptosis on renal injury in rats with acute paraquat poisoning. Mod J Integr Traditi Chin West Med 25: 2747-2750, 2016.
49. Evans CE, Peng Y, Zhu MM, Dai Z, Zhang X and Zhao YY: Rabeprazole promotes vascular repair and resolution of sepsis-induced inflammatory lung injury through HIF-1α. Cells 11: 1425, 2022.
50. Hughes T, Dijkstra KK, Rawlins EL and Hynds RE: Open questions in human lung organoid research. Front Pharmacol 13: 1083017, 2023.
51. Liberti DC and Morrisey EE: Organoid models: Assessing lung cell fate decisions and disease responses. Trends Mol Med 27: 1159-1174, 2021.
52. Bojkova D, Klann K, Koch B, Widera M, Krause D, Ciesek S, Cinatl J and Münch C: Proteomics of SARS-CoV-2-infected host cells reveals therapy targets. Nature 583: 469-472, 2020.
53. Riva L, Yuan S, Yin X, Martin-Sancho L, Matsunaga N, Pache L, Burgstaller-Muehlbacher S, De Jesus PD, Teriete P, Hull MV, *et al*: Discovery of SARS-CoV-2 antiviral drugs through large-scale compound repurposing. Nature 586: 113-119, 2020.
54. Okabe R, Chen-Yoshikawa TF, Yoshizawa A, Hirashima T, Saito M, Date H and Takebe T: Orthotopic foetal lung tissue direct injection into lung showed a preventive effect against paraquat-induced acute lung injury in mice. Eur J Cardiothorac Surg 58: 638-645, 2020.
55. Chen L, Yu T, Zhai Y, Nie H, Li X and Ding Y: Luteolin enhances transepithelial sodium transport in the lung alveolar model: Integrating network pharmacology and mechanism study. Int J Mol Sci 24: 10122, 2023.